

Linear Relative Pose Estimation Founded on Pose-only Imaging Geometry

Qi Cai¹, Xinrui Li¹, Yuanxin Wu^{1,*}
¹Shanghai Jiao Tong University

qicaiCN@gmail.com, physalis@sjtu.edu.cn, yuanx-wu@hotmail.com

Abstract

How to efficiently and accurately handle image matching outliers is a critical issue in two-view relative estimation. The prevailing RANSAC method necessitates that the minimal point pairs be inliers. This paper introduces a linear relative pose estimation algorithm for n ($n \geq 6$) point pairs, which is founded on the recent pose-only imaging geometry to filter out outliers by proper reweighting. The proposed algorithm is able to handle planar degenerate scenes, and enhance robustness and accuracy in the presence of a substantial ratio of outliers. Specifically, we embed the linear global translation (LiGT) constraint into the strategies of iteratively reweighted least-squares (IRLS) and RANSAC so as to realize robust outlier removal. Simulations and real tests of the Strecha dataset show that the proposed algorithm achieves relative rotation accuracy improvement of $2 \sim 10$ times in face of as large as 80% outliers.

1. Introduction

The popular pipeline in three-dimension (3D) visual computing, such as simultaneous localization and mapping (SLAM) and structure-from-motion (SfM), involves [24, 33]: 1) extracting, matching, and tracking image features; 2) removing image matching outliers through visual geometric constraints, such as the fundamental/essential/homography matrix equation; 3) estimating camera poses; and 4) reconstructing the 3D scene. While image feature extraction methods employ image Laplacian operators (like the SIFT [20], ORB [30] or SURF [1]) to identify interest points, matching outliers often occur in challenging scenarios such as those with insufficient lighting, occlusions, moving objects, and repetitive textures [15]. Those outliers would compromise the essential matrix [19] solution to two-view relative pose estimation. Additionally, when solving the essential equation, the two-view pose estimation encounters degeneracy problems [8, 18, 23, 32] (i.e. pure rotational motion or planar

structure).

Unfortunately, ensuring robustness to outliers remains a big challenge to 3D visual computing. For example, although the five-point algorithm can deal with the planar scene and pure rotational motion, it utilizes exactly five point pairs to construct five independent constraints of the essential matrix equation and to identify the true solution in the four-dimensional solution space [23, 32] by using an action matrix [32]. As a matter of fact, the essential equation under the planar scene or pure rotational motion has six independent constraints on the essential matrix for $n \geq 6$ point pairs [27, 28]. Consequently, the five-point algorithm lacks the constraint information of the essential matrix and is likely subject to multiple solutions among which the right one needs to identify (e.g. by using the Sampson distance of the co-planar constraint [11]).

Robust estimation methods such as RANSAC [10], LMedS [29], and M-estimation [13, 14] are essential to screen ubiquitous outliers. Specifically, RANSAC utilizes random sampling and consistency checks, combined with geometric constraints such as coplanar equations, to segregate inliers from outliers and to estimate the essential, fundamental or homography matrix. In the CVPR 2023 highlight paper, Peng *et al.* [25] introduced the GNC-IRLS method, a graduated non-convex strategy (GNC) for iteratively reweighted least-squares (IRLS), showcasing rapid convergence and accuracy in the context of 3D point registration.

The recent work [4] proposed a promising pose-only imaging geometry, which is equivalent to the classical multiple-view geometry and can be equivalently described using the linear global translation (LiGT) constraint. This pose-only representation has a significantly lower parameter space dimensionality, in contrast to the conventional bundle adjustment, by decoupling the 3D scene from the camera pose. Notably, the LiGT algorithm was embedded into the core library of OpenMVG [22] for global translation estimation, which is able to linearly solve global translations on given rotations of all views. It can handle some specific degenerate motions, such as local co-linearity, parallel rigidity and pure rotational motion [4].

*Corresponding author

The primary contributions of this paper include:

1. Propose a linear relative pose estimation algorithm (LiRP) based on the essential matrix equation to process all point pairs in one batch, enhancing the estimation accuracy and the capability of handling the degenerate planar scene and pure rotational motion.

2. Introduce the pose-only imaging geometry into the LiRP to screen outliers. The outlier identification is greatly improved by the re-weighted LiGT constraint’s residual thanks to the complete property of pose-only imaging geometry.

3. Incorporate RANSAC and the recent GNC-IRLS method into the LiRP for further robustness improvement.

The paper is organized as follows. Sec. 2 discusses the related works on two-view robust pose estimation. Sec. 3 presents the predefined mathematical notations. Sec. 4 reviews the constraints in two-view geometry and their residual statistics. The LiRP algorithm is proposed in Sec. 5. Sec. 6 elaborates on the combination of GNC-IRLS with RANSAC. Sec. 7 presents both simulation and real data test results. The paper is concluded in Sec. 8.

2. Related Works

2.1. Robust Estimation

In 1981, Fischler and Bolles introduced the RANSAC method [10], which subsequently became the mainstream outlier handling method in SLAM and SfM. The RANSAC method requires empirical parameters to be set according to specific estimation problems, such as the proportion of inliers to outliers and outlier detection error thresholds. Rousseeuw [29] introduced the LMedS method, which selects the optimal sub-sample using the minimum median deviation criterion with no need of presetting the threshold to distinguish inliers from outliers. The AC-RANSAC framework by Moisan *et al.* [21] adaptively updates RANSAC’s inlier and outlier parameters. Nonetheless, in 2017, Özyeşil *et al.* pointed out in [24] that the use of RANSAC could reduce the outlier mismatch rate to a higher yet acceptable level, for instance, 40% in offline applications; however, in real-time applications, the outlier ratio could be as high as 80% ~ 90%.

Furthermore, the robust M-estimator method [7, 13] is often employed in 3D vision such as pose graphs and bundle adjustments. It utilizes a loss function to weight the cost function, and aims to obtain robust solutions when faced with anomalies or non-normal data distributions. In two-view pose estimation, for example, a recent study [34] proposed a convex optimization-based solver for essential matrix estimation using all point pairs, which utilizes the M-estimator to handle outliers.

Another prevalent method for outlier treatment is based on the IRLS [12, 14], which reweights the conventional

least squares, highly susceptible to outliers, by using the observation residual. For instance, in global rotation averaging, Chatterjee *et al.* [5] utilized the IRLS scheme to enhance the estimation robustness. The recent study [25] proved the convergence of GNC-IRLS for outlier-robust estimation and proposed a smooth majorizer function and superlinear schedule update rule for IRLS.

2.2. Two-view Pose Constraints and Estimation

Nowadays, the mainstream methodologies of two-view relative pose estimation, for example those in such popular platforms as OpenMVG [22], COLMAP [31] and OpenGV [16], unexceptionally rely on the minimal matching point pairs and the essential matrix equation [11, 16, 19, 22, 32]. The advantage of the essential matrix coplanar equation is that it allows for a linear solution to the relative pose, but it loses the depth information and is an incomplete representation of two-view geometry [3, 4]. In fact, the relative pose estimation based on the essential matrix equation faces a number of challenges, such as multiple solutions, planar scenes, and pure rotational motion, among others [18, 23, 27, 28, 32, 34]. In 1996, Philip introduced a non-iterative algorithm to determine all essential matrices corresponding to five point pairs [26] and proposed a linear method for solving the essential matrix from six point pairs. In 2003, Pizarro *et al.* [28] introduced a six-point algorithm for robustly estimating the essential matrix, which remains effective even in the context of planar scenes. In 2004, Nister [23] employed the approach of solving the underdetermined group of coplanar equations to analyze the relationship between ternary polynomials and proposed a five-point algorithm for solving the essential matrix. In 2006, Stevenius and Nister [32] incorporated the Grobner base theory to further advance the five-point method.

Kneip *et al.* [18] believed that the traditional coplanar constraint had issues in expressing pure rotation, and then constructed a general coplanar constraint to describe two-view geometry. In specific, the authors utilized the Grobner base to solve the relative pose using the five-point method, and provided a method to identify the correct pose solution without 3D reconstruction. However, the shortcomings of the coplanar equation (loss of depth information and the presence of multiple solutions) has not been addressed until the work by Cai *et al.* [3] in 2019. The work introduced a pair of two-view pose-only constraints equivalent to the two-view imaging relationship, analytically decoupling the camera pose from the 3D point. Afterwards, the authors further extended the pose-only representation to multi-view imaging case, discovered a linear relationship between depth expression and translation, and came up with the LiGT constraint equivalent to the classical multi-view geometry [4].

3. Preliminaries and Notation

In this paper, we use the tilde symbol to denote the bearing vector form of a vector, i.e., $\tilde{\mathbf{a}} = \mathbf{a}/\|\mathbf{a}\|$, where $\|\mathbf{a}\|$ denotes the norm of the vector \mathbf{a} . The relative pose between the left and right views is represented by R and \mathbf{t} , respectively. The skew-symmetric matrix formed by any vector \mathbf{a} is denoted as $[\mathbf{a}]_{\times}$.

Assume that the left and right views correspond to camera coordinate systems C and C' centered at c and c' , respectively. Consider n 3D feature points, where $\mathbf{X}_i^C = (x_i^C, y_i^C, z_i^C)^T$ in the left camera system and $\mathbf{X}_i^{C'} = (x_i^{C'}, y_i^{C'}, z_i^{C'})^T$ in the right, the normalized image coordinates of the 3D point projected onto the left and right views are $\mathbf{x}_i = \mathbf{X}_i^C/z_i^C = (x_i, y_i, 1)^T$ and $\mathbf{x}'_i = \mathbf{X}_i^{C'}/z_i^{C'} = (x'_i, y'_i, 1)^T$, for $i = 1, \dots, n$. Here, z_i^C and $z_i^{C'}$ respectively represent the depths of the 3D points in the left and right views [4]. \mathbf{x}_i and \mathbf{x}'_i denote the normalized image coordinates of the corresponding point pair.

4. Two-view Constraints and Residuals

In the community of computer vision, the two-view geometry concerns the interrelation between two images of a specified scene, taken from two viewpoints. The two-view geometry is dictated by multiple different constraints that are crucial to a plethora of computer vision endeavors.

The 3D feature point in the two views are related via their relative pose by:

$$\mathbf{X}_i^{C'} = R\mathbf{X}_i^C + \mathbf{t}. \quad (1)$$

Then, the classical two-view imaging equation can be expressed as:

$$z_i^{C'} \mathbf{x}'_i = z_i^C R\mathbf{x}_i + \mathbf{t} \Leftrightarrow \mathbf{x}'_i = \lambda_i(R\mathbf{x}_i + s_i\mathbf{t}), \quad (2)$$

where $\lambda_i \triangleq z_i^C/z_i^{C'} \in \mathbb{R}^+$ and $s_i \triangleq 1/z_i^C \in \mathbb{R}^+$ represent unknown depth factors. Left-multiplying the equation on both sides by $\mathbf{x}_i'^T [\mathbf{t}]_{\times}$ to eliminate the depth factors, then we obtain the Longuet-Higgins's coplanar constraint [19]:

$$\mathbf{0} = \mathbf{x}_i'^T [\mathbf{t}]_{\times} \mathbf{x}'_i = \lambda_i \mathbf{x}_i'^T [\mathbf{t}]_{\times} R\mathbf{x}_i \Leftrightarrow \mathbf{x}_i'^T E\mathbf{x}_i = 0, \quad (3)$$

The derivation from Eq. (2) to Eq. (3) is irreversible, and it should be noted that Eq. (3) loses partial geometric imaging information, such as the forward intersection of projection rays [4]. In 2012, Kneip *et al.* [18] proposed a general coplanar equation to describe the relationship in two-view imaging geometry. It can be obtained by left-multiplying Eq. (2) by $\mathbf{t}^T [\mathbf{x}'_i]_{\times}$, that is:

$$\begin{aligned} \mathbf{0} &= \lambda_i \mathbf{t}^T [\mathbf{x}'_i]_{\times} (R\mathbf{x}_i + s_i\mathbf{t}) = \lambda_i \mathbf{t}^T [\mathbf{x}'_i]_{\times} R\mathbf{x}_i \\ &\Leftrightarrow \mathbf{t}^T (\mathbf{x}'_i \times R\mathbf{x}_i) = \mathbf{0}, \end{aligned} \quad (4)$$

which means that all vectors $\{\mathbf{x}'_i \times R\mathbf{x}_i | i = 1, \dots, n\}$ are located on a plane with the relative translation \mathbf{t} parallel to its normal vector. Define $B = (\mathbf{x}'_1 \times R\mathbf{x}_1, \dots, \mathbf{x}'_n \times R\mathbf{x}_n)^T$ and $M = BB^T$. According to Eq. (4), the B matrix is rank-deficient, i.e., the smallest eigenvalue of the M matrix satisfies the constraint [17, 18]:

$$\lambda_M(R) = 0, \quad (5)$$

Due to the irreversibility of the above derivation, the constraint still loses some geometric information. Furthermore, it can be shown that the Kneip's equation is equivalent to the essential equation Eq. (3), as detailed in the Appendix.A. Based on the coplanar equation constraint Eq. (3), the residual for a matched point pair is constructed in the form of bearing vectors as

$$v_i^E(R, \mathbf{t}, \tilde{\mathbf{x}}_i, \tilde{\mathbf{x}}'_i) = \|\tilde{\mathbf{x}}_i'^T E\tilde{\mathbf{x}}_i\|. \quad (6)$$

Unless otherwise specified, the residual vector formed by all point pairs will be denoted as \mathbf{v} . Kneip introduced a constraint for R optimization with $\lambda_M(R) = 0$ as shown in Eq. (5). However, the constraint in the form of smallest eigenvalue cannot be readily used to construct a residual for a point pair. In view of the fact that it is proven to be equivalent to the coplanar equation, only v^E will be further explored in the sequel. Note that the two-view imaging equation in Eq. (2) contains unknown depths, and thus it is not feasible to directly construct a residual either. Nonetheless, if the relative pose is determined, the gold-standard bundle adjustment error in two-view geometry can be formed by re-projection, that is,

$$v_i^{BA}(R, \mathbf{t}, \mathbf{X}_i^W, \mathbf{x}_i, \mathbf{x}'_i) = \left\| \frac{\boldsymbol{\epsilon}_i}{\mathbf{e}_3^T \boldsymbol{\epsilon}_i} - \mathbf{x}'_i \right\|, \quad (7)$$

where $\boldsymbol{\epsilon}_i = R(\mathbf{X}_i^W - \mathbf{t})$, \mathbf{X}_i^W is triangulated by the relative pose, and \mathbf{e}_3^T is the third row of the identity matrix. Using the bearing vector, another reprojection residual used by OpenGV [16] is

$$v_i^{OpenGV}(R, \mathbf{t}, \mathbf{X}_i^W, \tilde{\mathbf{x}}_i, \tilde{\mathbf{x}}'_i) = \|1 - \tilde{\boldsymbol{\epsilon}}_i^T \tilde{\mathbf{x}}'_i\|. \quad (8)$$

Recent studies [3, 4] proposed the pose-only imaging geometry by representing the depth factors as functions of poses, which is provably equivalent to the classical multi-view geometry. According to [3], the pairwise pose-only (PPO) constraint is given as

$$\frac{\|\mathbf{t} \times R\mathbf{x}_i\|}{\|\mathbf{x}'_i \times R\mathbf{x}_i\|} \mathbf{x}'_i = \frac{\|\mathbf{t} \times \mathbf{x}'_i\|}{\|\mathbf{x}'_i \times R\mathbf{x}_i\|} R\mathbf{x}_i + \mathbf{t}. \quad (9)$$

It should be highlighted that the depth factors are linearly related to translation [4], namely,

$$\begin{aligned} \frac{\|\mathbf{t} \times \mathbf{x}'_i\|}{\|\mathbf{x}'_i \times R\mathbf{x}_i\|} &= \frac{([R\mathbf{x}_i]_{\times} \mathbf{x}'_i)^T [\mathbf{x}'_i]_{\times} \mathbf{t}}{\theta_i^2} \triangleq \frac{1}{\theta_i^2} \mathbf{h}_i^T \mathbf{t}, \\ \frac{\|\mathbf{t} \times R\mathbf{x}_i\|}{\|\mathbf{x}'_i \times R\mathbf{x}_i\|} &= \frac{([R\mathbf{x}_i]_{\times} \mathbf{x}'_i)^T [R\mathbf{x}_i]_{\times} \mathbf{t}}{\theta_i^2} \triangleq \frac{1}{\theta_i^2} \mathbf{h}_i'^T \mathbf{t}, \end{aligned} \quad (10)$$

where $\theta_i = \|\mathbf{x}'_i \times R\mathbf{x}_i\|$. Substituting into Eq. (9) and left-multiplying $[\mathbf{x}'_i]_{\times}$, the LiGT constraint regarding the relative two-view translation is derived in [4] as:

$$\left([\mathbf{x}'_i]_{\times} R\mathbf{x}_i \mathbf{h}_i^T + \theta_i^2 [\mathbf{x}'_i]_{\times}\right) \mathbf{t} \triangleq L_i(R, \mathbf{x}_i, \mathbf{x}'_i) \mathbf{t} = 0 \quad (11)$$

Here, a two-view LiGT optimization (LiGTopt) is given by

$$\operatorname{argmin}_{(R, \mathbf{t})} \sum_i \|\tilde{L}_i \mathbf{t}\|, \quad (12)$$

where $\tilde{L}_i \triangleq L(R, \tilde{\mathbf{x}}_i, \tilde{\mathbf{x}}'_i)$. As seen from the derivation process from Eq. (3) to Eq. (4), both the PPO constraint and the above LiGT constraint encompass the coplanar essential matrix equation and the Kneip constraint. With these imaging constraints, two pose-only residuals can be formed, i.e.,

$$\begin{aligned} v_i^{LiGT}(R, \mathbf{t}, \tilde{\mathbf{x}}_i, \tilde{\mathbf{x}}'_i) &= \|\tilde{L}_i \mathbf{t}\|, \\ v_i^{PPO}(R, \mathbf{t}, \tilde{\mathbf{x}}_i, \tilde{\mathbf{x}}'_i) &= \|\tilde{\epsilon}_i - \tilde{\mathbf{x}}'_i\|, \end{aligned} \quad (13)$$

where $\epsilon_i = \|\mathbf{t} \times \tilde{\mathbf{x}}'_i\| R\tilde{\mathbf{x}}_i + \|\tilde{\mathbf{x}}'_i \times R\tilde{\mathbf{x}}_i\| \mathbf{t}$.

5. Six-Point Algorithm for Linear Relative Pose (LiRP)

Let Q represent the matrix to be solved in the essential equation Eq. (3), we have

$$\mathbf{x}_i^T Q \mathbf{x}_i = 0 \Leftrightarrow (\mathbf{x}_i^T \otimes \mathbf{x}_i^T) \mathbf{q} = 0 \triangleq A_i \mathbf{q} = 0, \quad (14)$$

where \mathbf{q} denotes the vectorized form of the matrix Q arranged column-wisely, and A_i is the i -th row vector of A matrix. Assume $\sigma_1 \geq \sigma_2 \geq \sigma_3$ are the three smallest singular values of matrix A , with their corresponding singular vectors \mathbf{q}_1 , \mathbf{q}_2 , and \mathbf{q}_3 . As $\operatorname{rank}(A) = 6$ in planar scene or pure rotational motion, the true solution of \mathbf{q} will be in the three-dimension solution space spanned by \mathbf{q}_1 , \mathbf{q}_2 , and \mathbf{q}_3 , i.e.,

$$\mathbf{q} = a\mathbf{q}_1 + b\mathbf{q}_2 + c\mathbf{q}_3, \quad (15)$$

where a , b , and c are coefficients to be determined. The solution \mathbf{q} is determined up to a scale. Subsequently, the determination of these coefficients can be discussed by two cases:

Case (1): Let $c = 1$, then the values of a and b can be determined such that Q is an essential matrix satisfying the Demazure constraint [9]:

$$QQ^T Q - \frac{1}{2} \operatorname{trace}(QQ^T) Q = 0 \Leftrightarrow B\mathbf{y} = 0, \quad (16)$$

where B is a 9×10 matrix constructed from \mathbf{q}_1 , \mathbf{q}_2 , and \mathbf{q}_3 , and $\mathbf{y} = (a^3, a^2b, ab^2, b^3, a^2, ab, b^2, a, b, 1)^T$. Assuming that the first four columns form a submatrix B_1 and the remaining columns constitute a submatrix B_2 , that is, $B =$

$(B_1|B_2)$. By left multiplying Eq. (16) with the pseudo-inverse of B_1 , denoted as B_1^+ , we obtain $(I_{4 \times 4} | M_{4 \times 6}) \mathbf{y} = 0$. The left-side structure of the above equation can be illustrated as in Tab. 1, of which the first row lists the monomial elements of \mathbf{y} , the horizontal bars "-" represent specific values of M , and other blank entries are 0s. Notably, each monomial of third order in \mathbf{y} can be expressed as linear combinations of those of lower orders in the same row. In this regard, $(I|M)\mathbf{y} = 0$ gives rise to the equations $C_1 \mathbf{g} = a\mathbf{g}$ and $C_2 \mathbf{g} = b\mathbf{g}$ of eigensystem form, where $\mathbf{g} = (a^2, ab, b^2, a, b, 1)^T$. Therefore, by determining the eigenvectors of 6-by-6 action matrices C_1 and C_2 , as many as 12 potential solution vectors for \mathbf{g} can be derived. The coefficients a and b can be directly determined from the last three elements of each solution vector, specifically, $a = g_4/g_6$ and $b = g_5/g_6$. In this scenario, we obtain 12 candidate solutions for \mathbf{q} , denoted as \mathbf{q}_s .

a^3	a^2b	ab^2	b^3	a^2	ab	b^2	a	b	1
1				-	-	-	-	-	-
	1			-	-	-	-	-	-
		1		-	-	-	-	-	-
			1	-	-	-	-	-	-

Table 1. Polynomial system.

Case (2). If $c = 0$, then we deduce $\mathbf{q} = a\mathbf{q}_1 + b\mathbf{q}_2$. Analogously, setting $b = 1$ and only a needs to be determined. Considering the property that the determinant of the essential matrix is zero, a polynomial in terms of a can be constructed by

$$\det(Q) = 0 \Leftrightarrow \mathbf{d}^T \mathbf{z} = 0, \quad (17)$$

where $\mathbf{z} = (a^3, a^2, a, 1)^T$. In analogy to Case (1), three candidate solutions for \mathbf{q} can be derived, say \mathbf{q}'_s . Setting $b = 0$, \mathbf{q}_1 also emerges as a potential solution. Taking into account different solution sequences, \mathbf{q}_2 and \mathbf{q}_3 can similarly be considered as candidate solutions.

In summary, the above analysis yields 18 candidate solutions for $\hat{\mathbf{q}} = (\mathbf{q}_s, \mathbf{q}'_s, \mathbf{q}_1, \mathbf{q}_2, \mathbf{q}_3)$. Each candidate solution can be decomposed into four relative pose solutions [11]. With the aid of the relative pose identification's inequality strategy revealed in [3], that is to say, $M_1(R) > 0$ and $M_2(R, \mathbf{t}) > 0$ therein, eighteen candidate solutions of the essential matrix can be processed to yield the same number of relative pose candidate solutions. Subsequently, the identification will further rely on minimizing v^{PPO} , to be explained in next section.

6. Brief Summary of GNC-RANSAC method

The recent GNC-base IRLS method [25] alternates between optimizing a smooth majorizer function and increasing a

Algorithm 1 Weighted LiRP Algorithm

Require: point pairs $\{(\tilde{\mathbf{x}}_1, \tilde{\mathbf{x}}'_1), \dots, (\tilde{\mathbf{x}}_n, \tilde{\mathbf{x}}'_n)\}$, (optional) weights w

Ensure: relative rotations R and translations t

- 1: construct weighted A matrix $\leftarrow A_i = w_i(\tilde{\mathbf{x}}_i^T \otimes \tilde{\mathbf{x}}_i'^T)$
 - 2: obtain $\mathbf{q}_1, \mathbf{q}_2, \mathbf{q}_3 \leftarrow$ SVD decomposition of A matrix
 - 3: compute B matrix by Eq. (16)
 - 4: obtain M matrix by left multiplying $B_1^+ B$
 - 5: construct $C_1, C_2 \leftarrow M$
 - 6: $\mathbf{q}_s \leftarrow$ eigenvectors of C_1, C_2
 - 7: $\mathbf{q}'_s \leftarrow$ solve polynomial by Eq. (17)
 - 8: $\hat{\mathbf{q}} \leftarrow \mathbf{q}_s, \mathbf{q}'_s, \mathbf{q}_1, \mathbf{q}_2, \mathbf{q}_3$
 - 9: $R, t \leftarrow \hat{\mathbf{q}}$
-

parameter μ at each iteration, which is designed to accelerate convergence and yield stable outcomes. The majorizer function, denoted as $q(v_i, \mu)$, represents a shifted version of the objective function $\rho(v_i)$, which is to be minimized. The parameter μ controls the tradeoff between accuracy and robustness. By alternately updating the majorizer function and increasing μ , GNC [2] aims to find a stationary point of the objective function to reach convergence. In general IRLS problems, the scale-invariant issue is often considered. Let σ denote the standard deviation of the sample. In this paper, based on the recommendation of Huber [14], we use the median of absolute deviations to determine σ , i.e., $\sigma = 1.4826 \times \text{med}|\hat{v}_i - \text{med}(\hat{v}_i)|$. By integrating the GNC-IRLS with the LiRP algorithm, we developed a robust relative pose estimation method, as shown in Algorithm 2. For instance, with 30 point pairs, it can resist nearly 40% outlier fraction. However, for higher outlier fractions, the RANSAC scheme is still needed to increase robustness, as seen in Algorithm 3. Compared to the standard RANSAC method, our robust relative pose estimation algorithm for fitting model relaxes the requirement that all sub-samples must consist entirely of inliers. Instead, it ensures that the outlier fraction in sub-samples does not exceed a certain threshold, such as 40%. This approach makes it easier to find suitable sub-samples at higher outlier fractions.

7. Experiments

The global translation has been well solved by the LiGT algorithm that is linear in nature and capable to produce nearly optimal global translation if provided excellent input of rotations [4]. Unlike traditional methods [23, 28, 32, 34] that have mostly emphasized the accuracy and robustness of relative translation, the current work focuses on the performance of relative rotation estimation.

In both simulation and real testing, the sampling size for GNC-RANSAC is set to $n_s = 30$ and the maximum iteration of RANSAC is consistently set to 50 for all algorithms

Algorithm 2 GNC-IRLS Pose Estimation Algorithm

Require: Point pairs $\{(\tilde{\mathbf{x}}_1, \tilde{\mathbf{x}}'_1), \dots, (\tilde{\mathbf{x}}_n, \tilde{\mathbf{x}}'_n)\}$, stop threshold ϵ_0 , maximum iteration n_{iter}

Ensure: The model parameters R, t

- 1: Initialize $\epsilon^{(0)}, \mu^0$, and weights $w^{(0)}$,
 - 2: $converged \leftarrow$ false
 - 3: **for** $k \leftarrow 0$ to $n_{iter} - 1$ **do**
 - 4: Obtain $R^{(k)}, t^{(k)}$ with $w^{(k)}$ by Algorithm 1
 - 5: Compute residual vector v^{LiGT} by Eq. (13)
 - 6: $\sigma^{(k)} \leftarrow 1.4826 \cdot \text{median}(|v^{LiGT}|)$
 - 7: $c^{(k)} \leftarrow 5.54 \cdot \sigma^{(k)}$
 - 8: $w^{(k+1)} \leftarrow$ Update weights by $v^{LiGT}, c^{(k)}$, and $\mu^{(k)}$ according to [25]
 - 9: $\epsilon^{(k+1)} \leftarrow \sum w_i^{(k+1)} v_i^{LiGT}$
 - 10: **if** $|\epsilon^{(k+1)} - \epsilon^{(k)}| < \epsilon_0$ **then**
 - 11: $converged \leftarrow$ true
 - 12: **exit loop**
 - 13: **end if**
 - 14: Update $\mu^{(k+1)}$ by super-linear schedule [25]
 - 15: **end for**
-

Algorithm 3 GNC-RANSAC Algorithm

Require: point pairs $P = \{(\tilde{\mathbf{x}}_1, \tilde{\mathbf{x}}'_1), \dots, (\tilde{\mathbf{x}}_n, \tilde{\mathbf{x}}'_n)\}$, stop threshold ϵ_0 , sample size n_s, n_{iter} , inlier threshold θ

Ensure: the model parameters R, t

- 1: $n_{maxinliers} \leftarrow 0; R_{best}, t_{best} \leftarrow \emptyset$
 - 2: **for** $k \leftarrow 0$ to $n_{iter} - 1$ **do**
 - 3: $P_s \leftarrow$ randomly select n_s sample from P
 - 4: $R_s, t_s \leftarrow$ fit model using Algorithm 2 with P_s
 - 5: $v^{LiGT} \leftarrow$ obtain residual vector by Eq. (13) for P
 - 6: $P_{inliers} \leftarrow v^{LiGT}, \theta$
 - 7: **if** $|P_{inliers}| > n_{maxinliers}$ **then**
 - 8: $n_{maxinliers} \leftarrow |P_{inliers}|$
 - 9: $R_{best}, t_{best} \leftarrow R_s, t_s$
 - 10: $P_{best} \leftarrow P_{inliers}$
 - 11: **end if**
 - 12: **end for**
 - 13: $R, t \leftarrow$ fit model using Algorithm 2 with P_{best}
-

under investigation.

7.1. Synthetic Experiment

The synthetic scenarios are of two types: 1) a normal scenario generated by using the OpenGV's code to construct 3D feature points and camera poses of two views, retaining only those bearing vectors satisfying chirality constraints (see Fig. 1); 2) a planar scenario intentionally generated to examine the algorithm's behavior in a planar scene. The synthetic experiment was conducted in the Ubuntu 18.04 environment running on a single core. Monte Carlo tests

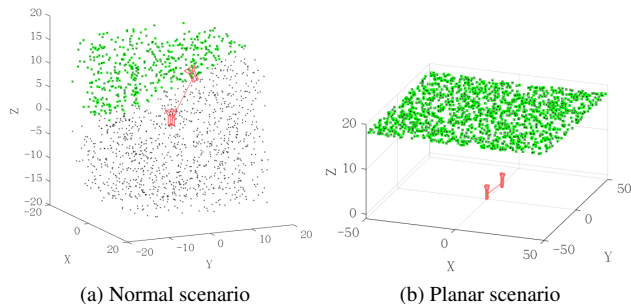


Figure 1. Simulation of two-view structure and 3D feature points. The green nodes represent 3D points that conform to chirality constraints, and the black nodes represent 3D points otherwise. The two red cameras represent the pose of the two views. The red line indicates the displacement baseline.

were repeated 500 times. The image matching outliers were generated by a predetermined outlier fraction. Before running the experiment, we categorized the compared algorithms into two groups: the first group includes initial relative pose estimation methods, including the Pizarro’s 6pt algorithm [28], the LiRP algorithm, and 5pt [32] / 7pt [11] / 8pt [11] algorithms supported by OpenGV. The second group comprises optimization techniques, including the N -point method (Npt) [34], eigensolver [17] / nonlinear optimization [16] in OpenGV, BA [11], and the LiGT optimization.

7.1.1 Robustness of relative pose estimation

Unlike the RANSAC method, IRLS typically requires reweighting almost all matches. The Stewenius method, a well-established approach for estimating relative pose, is traditionally employed for sets of five matching points and can also be extended to handle more than five pairs of points ($n \geq 6$) [32]. It is widely recognized that both the 7pt and 8pt methods exhibit planar degeneracy. It has been pointed out [28, 32] that the linear 6-point algorithm [26] also suffers from planar degeneracy, and the Pizarro’s 6pt method has been found to be prone to instability in solutions.

The noise-free experiment in Tab. 2 throws lights on the theoretical limitation of the Stewenius method when addressing n -point pairs ($n = 30$ herein) within planar configurations. Specifically, under the planar scene with a noise-free condition, the action matrix constructed by using the Stewenius method [32] for n point pairs has repeated eigenvalues. The multiple eigenvectors corresponding to the repeated eigenvalues lead to infinite solutions of essential matrix. We utilized an indicator $d_{\min} = \min_{i,j} \{|\lambda_i - \lambda_j|\}$ to quantify the minimum distance between the eigenvalues of the action matrix. In the case of a noise-free planar scene, the Stewenius method’s d_{\min} is zero, signifying the presence of

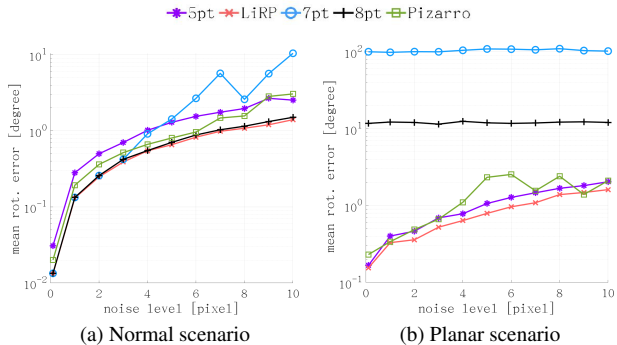


Figure 2. Noise test results of initial relative pose estimation methods.

duplicate eigenvalues. The rotation accuracy of $2.79e^{-2}$ indicates the above-mentioned limitation. Fortunately, when point pairs are subject to 0.1 pixel noise, this limitation is largely mitigated. The result in Tab. 2 also reveals the planar degenerate problem for the N -point method [34]. In contrast, the LiRP algorithm consistently achieved the best accuracy in both normal and planar scenes, maintaining d_{\min} above acceptable thresholds. The LiRP algorithm’s rotation accuracy further confirms the absence of planar case limitations.

Subsequently, we conducted tests to evaluate the impact of noises on relative pose estimation methods for n point pairs problem, see Figs. 2 and 3. We compare the performance without outliers across a spectrum of noise levels for 30 point pairs, which were incremented from 0 to 10 pixels in steps of one pixel.

In normal scenarios, as evidenced by Fig. 2a and Fig. 3a, the LiRP estimation and the LiGT optimization both demonstrate outstanding accuracy. Notably, LiRP achieves the lowest mean rotational error, particularly as noise levels increase, in stark contrast to the 5pt and Pizarro’s 6pt methods. Moreover, LiRP’s rotational accuracy not only competes with but often surpasses that of BA optimization and is on par with the majority of other optimization techniques. Concurrently, LiGT optimization upholds the highest standard of rotational accuracy, even as noise levels escalate. Note that the Npt method are prone to degenerate problems in planar scenes, as shown in Fig. 3b.

7.1.2 Selection of Optimal Residual Statistics

In the sequel, we compared the optional residual statistics in Sec. 4 and selected the optimal one to be combined with the GNC scheme in Algorithm 2. With image noise fixed at 1 pixel, Fig. 4 displays the mean error results of different residual statistics across different outlier fraction ratios for $n = 30$. We use ‘MS-TLS’ to denote the majorization and superlinear GNC schedule for truncated least-

Table 2. Structure degenerate problem for relative rotation estimation. The pair (x,y) represents 'x' as the mean rotation error and 'y' as the minimum distance d_{\min} between the eigenvalues of the action matrix. The symbol '-' signifies that no data is provided. The labels (5) and (n) in column headers correspond to results estimated using five and n point pairs, respectively. The multiple solutions of essential matrix herein are identified using the true essential matrix.

Scenes	Noise Pixel	5pt (5) [32]	5pt (m) [32]	LiRP (m)	Npt (m) [34]
Planar	0	(0, $4.19e^{-1}$)	($2.79e^{-2}$, $1.08e^{-15}$)	(0, 1.44)	($3.48e^{-2}$, -)
	0.1	($3.36e^{-3}$, $4.45e^{-1}$)	($2.75e^{-4}$, $1.40e^{-4}$)	($2.54e^{-4}$, 1.28)	($4.38e^{-2}$, -)
Normal	0	(0, $2.27e^{-1}$)	(0, $7.80e^{-3}$)	(0, 1.23)	(0, -)
	0.1	($2.58e^{-3}$, $3.10e^{-1}$)	($5.47e^{-4}$, $7.56e^{-3}$)	($2.03e^{-4}$, 1.32)	($2.16e^{-4}$, -)

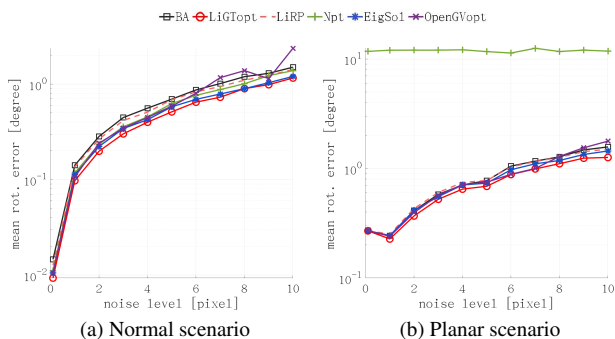


Figure 3. Noise test results of optimization methods, which are all initialized by LiRP.

squares loss [25]. In each subplot, we have incorporated the RANSAC-based 5pt method in OpenGV as comparison benchmark.

From Fig. 4, it is obvious that the MS-TLS strategy of utilizing v^{LiGT} as the re-weighted iterative residual statistic yields the highest rotation accuracy, which ensures that the rotation error remains less than 1° for up to 40% outlier fractions in normal scene (see Fig. 4a) and 30% outlier fractions in planar scene (see Fig. 4b).

Considering the results from Fig. 4, it is evident that using v^{LiGT} as the residual statistics for weighting is most appropriate in relative rotation estimation.

7.1.3 Results of the GNC-RANSAC Scheme

To obtain a reasonable rotation estimation with the outlier fraction over 50%, we proposed a fusion strategy by combining GNC and RANSAC. We set the image noise to 1 pixel, chose $n_s = 30$, and conducted tests in both normal and planar scenarios for $n = 300$. The simulation results are illustrated in Fig. 5. For outlier fractions from 50% to 80%, our strategy consistently ensured high-accuracy rotation results. Remarkably, at a 80% outlier fraction, it significantly outperformed other strategies in both normal and planar scenarios, with an accuracy improvement of nearly two orders of magnitude. At lower outlier fractions, our strategy maintained a considerable lead in rotation accuracy.

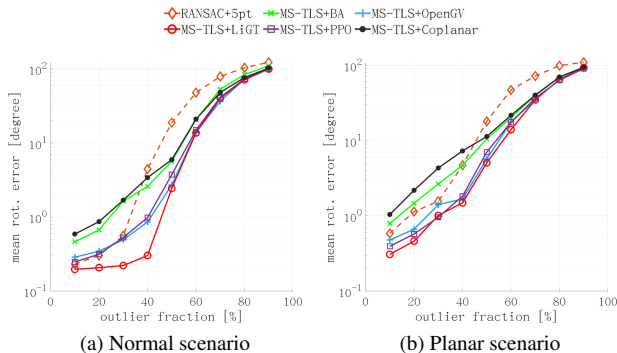


Figure 4. Robustness test for different residuals. All variants of MS-TLS utilize LiRP for relative rotation. The dashed line represents the benchmark result (RANSAC+5pt) provided by OpenGV.

Note that the rotation accuracy of robust-Npt is not consistent with the reported result in [34] because of a simulation issue of chirality therein. Please see Appendix.B for details.

7.2. Real Data Experiment with Strecha

For each Strecha data, we obtained raw pair matches between two views by using SIFT [20] and the Cascade hashing [6] for feature extraction and matching, respectively. Then, we only processed those raw point pairs that is larger than 30 in number. Specifically, relative rotations between i -th and j -th views, namely $\hat{R}_{i,j}$, were obtained by using OpenGV's RANSAC and GNC-RANSAC schemes. The angular distance between these estimates and the true relative rotations $R_{i,j}$ was computed by

$$\epsilon_{i,j} = \arccos \left(\frac{\text{trace} \left(R_{i,j}^\top \hat{R}_{i,j} \right) - 1}{2} \right). \quad (18)$$

Regarding relative rotation accuracy in Tab. 3, the GNC-RANSAC method generally is superior to OpenGV by $2 \sim 3$ times across the Strecha dataset. Particularly, the GNC-RANSAC exhibits a median error ϵ_{med} of 0.044 for Herz-Jesus-P8, which is notably lower than OpenGV's 0.096. However, for Castle-P30, there exists a significant number of mismatches because of repeated texture, as

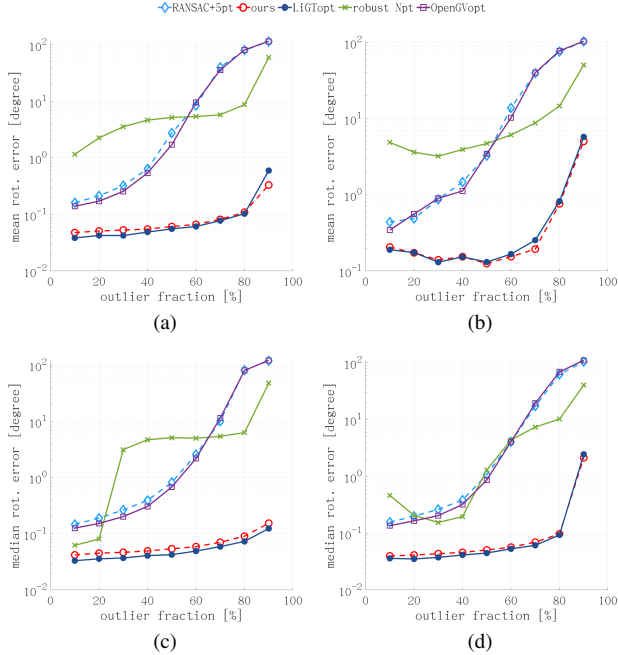


Figure 5. Accuracy of the GNC-RANSAC fusion scheme as compared with state-of-art methods. LiGTopt is optimized based on our GNC-RANSAC scheme, and OpenGVopt is optimized based on OpenGV’s RANSAC+5pt. The first and second columns are for normal scenes and planar scenes, respectively. Dashed and solid lines represent the initial and optimization relative rotation results, respectively.

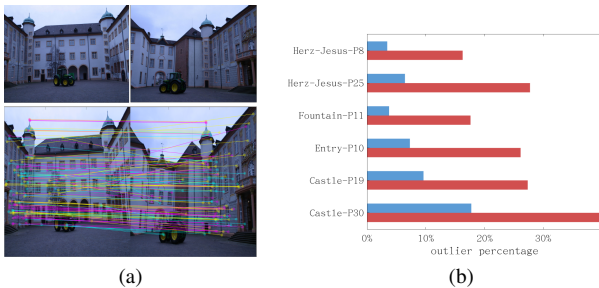


Figure 6. (a) Demo of repeated texture and the (point/view) pair outliers in Castle-P30. (b) Identified outlier percentage for Strecha data (blue for OpenGV, red for GNC-RANSAC).

shown in Fig. 6a. Although the proposed GNC-RANSAC method can handle a great portion of those mismatches (see Fig. 6b), there are still considerable percentage wrongly taken as inliers in Castle-P30 that results in relatively larger errors than other data. Fig. 6b compared the outlier percentage for all Strecha data identified by OpenGV and GNC-RANSAC schemes. The number of identified outliers by GNC-RANSAC is 2 ~ 4 times of that by OpenGV, which partially explains the higher rotation accuracy of the former.

Given the relative rotations, Fig. 7 exemplifies the global

Table 3. Relative rotation accuracy (degree) comparison.

Data	OpenGV		GNC-RANSAC	
	ϵ_{mean}	ϵ_{med}	ϵ_{mean}	ϵ_{med}
Herz-Jesus-P8	0.125	0.096	0.072	0.044
Herz-Jesus-P25	0.364	0.162	0.214	0.078
Fountain-P11	0.149	0.101	0.0647	0.0480
Entry-P10	0.748	0.180	0.0412	0.0367
Castle-P19	2.535	0.468	0.449	0.100
Castle-P30	2.385	0.365	1.949	0.089

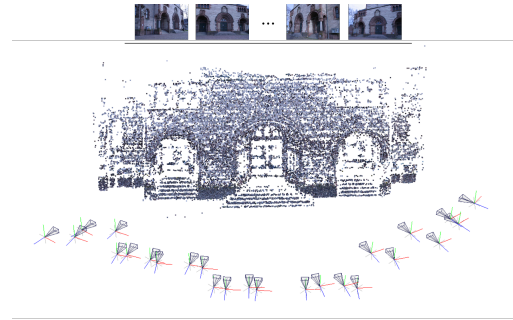


Figure 7. Global camera poses and 3D points in Herz-Jesus-P25 obtained by the pipeline of global rotation averaging, global translation estimation, and analytical reconstruction.

poses and 3D points of Herz-Jesus-P25 reconstructed by the pipeline of Chatterjee’s global rotation averaging [5], LiGT for global translation, and then analytical reconstruction [4]. The apparently high quality of 3D reconstruction, at the absence of global optimization, indirectly verifies the satisfying relative rotation accuracy.

8. Conclusions

This paper introduces a linear relative pose estimation algorithm to handle planar degenerate scenes for $n \geq 6$ point pairs. The proposed algorithm utilizes the pose-only constraint to construct the residual of identifying the image matching outliers, integrated with GNC-IRLS and RANSAC for improved robustness. Simulations and real tests of the Strecha dataset show that the proposed algorithm achieves relative rotation accuracy improvement of 2 ~ 10 times in face of as large as 80% outliers. Our future work will focus on the strategy of refining/replacing IRLS and RANSAC, for example by removing the manually-tuned parameters.

A. Equivalence Proof of Kneip’s and Essential Equations

Here, we provide an equivalence proof for Kneip’s constraint in Eq. (5) and essential equation.

Proposition: In two-view geometry, the Kneip’s constraint is equivalent to the essential equation.

Proof:

a) Sufficiency Proof: Assume a matrix $B = (\mathbf{x}'_1 \times R\mathbf{x}_1, \dots, \mathbf{x}'_n \times R\mathbf{x}_n)^T \triangleq (\mathbf{b}_1, \dots, \mathbf{b}_n)^T$, where

$$\mathbf{b}_i^T = \text{vec}(R)^T (x_i [\mathbf{x}'_i]_{\times} \quad y_i [\mathbf{x}'_i]_{\times} \quad [\mathbf{x}'_i]_{\times})^T. \quad (19)$$

The operator $\text{vec}()$ denotes the vectorization of a matrix. Let $R = (\mathbf{r}_1 \quad \mathbf{r}_2 \quad \mathbf{r}_3)$ and substituting it into the above equation

$$\begin{aligned} \mathbf{b}_i^T &= -x_i \mathbf{r}_1^T [\mathbf{x}'_i]_{\times} - y_i \mathbf{r}_2^T [\mathbf{x}'_i]_{\times} - \mathbf{r}_3^T [\mathbf{x}'_i]_{\times} \\ &= (x_i \mathbf{x}'_i{}^T \quad y_i \mathbf{x}'_i{}^T \quad \mathbf{x}'_i{}^T) \begin{pmatrix} [\mathbf{r}_1]_{\times} \\ [\mathbf{r}_2]_{\times} \\ [\mathbf{r}_3]_{\times} \end{pmatrix} \\ &\triangleq (\mathbf{x}_i^T \otimes \mathbf{x}'_i{}^T) G \\ &\triangleq \mathbf{a}_i^T G. \end{aligned} \quad (20)$$

According to the Kneip's constraint: only the correct R will cause the matrix B to be rank deficient. That is to say, only the correct rotation matrix R results in a non-zero vector $\mathbf{k} = (k_1, k_2, k_3)^T \in \mathbb{R}^{3 \times 1}$ satisfying

$$\mathbf{a}_i^T G \mathbf{k} = 0. \quad (21)$$

Considering the specific form of G matrix, we have

$$-G\mathbf{k} = - \begin{pmatrix} [\mathbf{r}_1]_{\times} \\ [\mathbf{r}_2]_{\times} \\ [\mathbf{r}_3]_{\times} \end{pmatrix} \mathbf{k} = \begin{pmatrix} [\mathbf{k}]_{\times} \mathbf{r}_1 \\ [\mathbf{k}]_{\times} \mathbf{r}_2 \\ [\mathbf{k}]_{\times} \mathbf{r}_3 \end{pmatrix} \triangleq \text{vec}(Q), \quad (22)$$

where $Q = ([\mathbf{k}]_{\times} \mathbf{r}_1 \quad [\mathbf{k}]_{\times} \mathbf{r}_2 \quad [\mathbf{k}]_{\times} \mathbf{r}_3) = [\mathbf{k}]_{\times} R$. Therefore,

$$(\mathbf{x}_i^T \otimes \mathbf{x}'_i{}^T) \text{vec}(Q) = \mathbf{x}_i^T [\mathbf{k}]_{\times} R \mathbf{x}_i = 0. \quad (23)$$

Substituting Eq. (2) into the above, we have

$$(R\mathbf{x}_i + s_i \mathbf{t})^T [\mathbf{k}]_{\times} R \mathbf{x}_i = \mathbf{t}^T [\mathbf{k}]_{\times} R \mathbf{x}_i = 0. \quad (24)$$

Since the above equation holds for any normalized image coordinates \mathbf{x}_i , it indicates $\mathbf{k} = \mathbf{t}$ (up to a scale), hence $\mathbf{x}_i^T E \mathbf{x}_i = 0$ is valid.

b) Necessity Proof: According to the essential equation in Eq. (3), we have $(\mathbf{x}_i^T \otimes \mathbf{x}'_i{}^T) \text{vec}(Q) = 0$, where Q denotes the solution to the essential equation. According to [3] and considering Eq. (2),

$$(\mathbf{x}_i^T \otimes (\mathbf{x}'_i^T \quad s_i)) (I_3 \otimes (R \quad \mathbf{t})^T) \text{vec}(Q) = 0 \quad (25)$$

For all point pairs, we have

$$L\mathbf{y} = \mathbf{0} \quad (26)$$

where

$$L \triangleq \begin{pmatrix} \mathbf{x}_1^T \otimes (\mathbf{x}'_1^T \quad s_1) \\ \vdots \\ \mathbf{x}_n^T \otimes (\mathbf{x}'_n^T \quad s_n) \end{pmatrix}, \quad (27)$$

and

$$\mathbf{y} \triangleq (I_3 \otimes (R \quad \mathbf{t})^T) \text{vec}(Q). \quad (28)$$

Expanding the L matrix, we have

$$L = \begin{pmatrix} x_1^2 & x_1 y_1 & x_1 & x_1 s_1 & y_1 x_1 & y_1^2 & y_1 & y_1 s_1 & x_1 & y_1 & 1 & s_1 \\ \vdots & \vdots & \vdots & \vdots & \vdots & \vdots & \vdots & \vdots & \vdots & \vdots & \vdots & \vdots \\ x_n^2 & x_n y_n & x_n & x_n s_n & y_n x_n & y_n^2 & y_n & y_n s_n & x_n & y_n & 1 & s_n \end{pmatrix}. \quad (29)$$

As columns 2, 3, and 7 are respectively equal to 5, 9, and 10, we have $\text{rank}(L) \leq 9$. Let $A = L (I_3 \otimes (R \quad \mathbf{t})^T)$, we have $\text{rank}(A) \leq 9$. Therefore, when $n \geq 9$ the homogeneous equation in Eq. (26) has three linearly independent special solutions

$$\begin{aligned} \xi_1 &= (0 \ 1 \ 0 \ 0 \ -1 \ 0 \ 0 \ 0 \ 0 \ 0 \ 0)^T, \\ \xi_2 &= (0 \ 0 \ 1 \ 0 \ 0 \ 0 \ 0 \ -1 \ 0 \ 0 \ 0)^T, \\ \xi_3 &= (0 \ 0 \ 0 \ 0 \ 0 \ 1 \ 0 \ 0 \ -1 \ 0 \ 0)^T. \end{aligned} \quad (30)$$

The solution space of \mathbf{y} is given by

$$\mathbf{y} = (I_3 \otimes (R \quad \mathbf{t})^T) \text{vec}(Q) = (\xi_1 \quad \xi_2 \quad \xi_3) \mathbf{c}, \quad (31)$$

where $\mathbf{c} = (c_1, c_2, c_3)^T$ is a non-zero real vector. By using the Kronecker product equality

$$(I_3 \otimes (R \quad \mathbf{t})^T) \text{vec}(Q) = \text{vec}((R \quad \mathbf{t})^T Q), \quad (32)$$

we can obtain

$$Q = R[\mathbf{c}]_{\times} = [\mathbf{k}]_{\times} R, \quad (33)$$

where $\mathbf{k} = R\mathbf{c}$. It means that there exists at least one non-zero vector $\mathbf{k} = (k_1, k_2, k_3)^T \in \mathbb{R}^{3 \times 1}$ satisfying $Q = [\mathbf{k}]_{\times} R$, which is $\text{vec}(Q) = G\mathbf{k}$. Substituting into the essential equation in Eq. (3), we have $\mathbf{a}_i^T G \mathbf{k} = \mathbf{b}_i^T \mathbf{k} = 0$, i.e., matrix B must be rank deficient, and hence the essential equation implies the Kneip constraint.

In summary, the Kneip's constraint and the essential equation are equivalent. Q.E.D.

B. Performance of Robust N-point Method

The rotational accuracy of the robust N-point method, as presented in Sec. 7, does not align with the results reported by Zhao [34]. In our robustness experiments, we employed 300 point pairs satisfying the chirality constraint, with each pair generated at a noise level of 1 pixel, subject to Gaussian distribution. We fixed the maximum translation magnitude at 2 units and had the depth of 3D points ranged from 4 to 18. An attitude perturbation of 0.5 degrees was applied. To ensure reliability, we repeated the experiment 500 times. For the RANSAC algorithm, we used the default OpenGV settings.

In contrast, the point pairs used in the robust N-point method [34] were generated from OpenGV's simulations

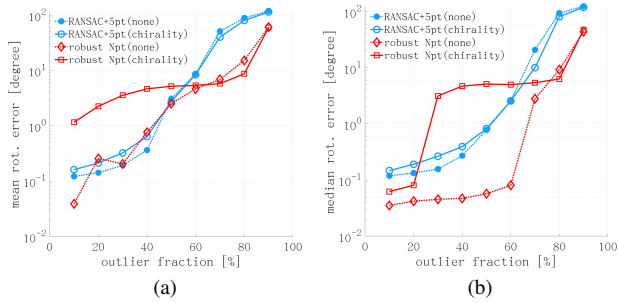


Figure 8. Performance of robust Npt and RANSAC+5pt in cases of disregarding or considering the chirality constraint. We use 'none' to denote the point pair generation disregarding the chirality constraint, and 'chirality' to represent the generation considering the chirality constraint.

that did not consider the chirality constraint. Thus, we compared the performance of robust N-point method in cases of disregarding or considering the chirality constraint in Fig. 8. In the case of disregarding the chirality constraint, the mean and median errors of the robust N-point method significantly reduced. In other words, the results reported in [34] are not objective in that those simulated point pairs disregarding the chirality constraint should not have been taken into account. Finally, in cases with 90% outlier fraction, as depicted in Fig. 8, the rotation errors of OpenGV's RANSAC+5pt method are around 10^2 degrees, which also contrasts with the result of 10 degrees in [34].

References

- [1] Herbert Bay, Andreas Ess, Tinne Tuytelaars, and Luc Van Gool. Speeded-up robust features (SURF). *Computer vision and image understanding*, 110(3):346–359, 2008. 1
- [2] Andrew Blake and Andrew Zisserman. *Visual reconstruction*. MIT press, 1987. 5
- [3] Qi Cai, Yuanxin Wu, Lilian Zhang, and Peike Zhang. Equivalent constraints for two-view geometry: Pose solution/pure rotation identification and 3d reconstruction. *International Journal of Computer Vision*, 127:163–180, 2019. 2, 3, 4, 9
- [4] Qi Cai, Lilian Zhang, Yuanxin Wu, Wenxian Yu, and Dewen Hu. A pose-only solution to visual reconstruction and navigation. *IEEE Transactions on Pattern Analysis and Machine Intelligence*, 45(1):73–86, 2021. 1, 2, 3, 4, 5, 8
- [5] Avishek Chatterjee and Venu Madhav Govindu. Robust relative rotation averaging. *IEEE Transactions on Pattern Analysis and Machine Intelligence*, 40(4):958–972, 2017. 2, 8
- [6] Jian Cheng, Cong Leng, Jiayang Wu, Hainan Cui, and Hanqing Lu. Fast and accurate image matching with cascade hashing for 3d reconstruction. In *Proceedings of the IEEE/CVF Conference on Computer Vision and Pattern Recognition (CVPR)*, pages 1–8, 2014. 7
- [7] DQF De Menezes, Diego Martinez Prata, Argimiro R Secchi, and José Carlos Pinto. A review on robust M-estimators

- for regression analysis. *Computers & Chemical Engineering*, 147:107254, 2021. 2
- [8] Peter Decker, Dietrich Paulus, and Tobias Feldmann. Dealing with degeneracy in essential matrix estimation. In *IEEE International Conference on Image Processing*, pages 1964–1967, 2008. 1
- [9] Olivier Faugeras. *Three-dimensional computer vision: a geometric viewpoint*. MIT press, 1993. 4
- [10] Martin A Fischler and Robert C Bolles. Random sample consensus: a paradigm for model fitting with applications to image analysis and automated cartography. *Communications of the ACM*, 24(6):381–395, 1981. 1, 2
- [11] Richard Hartley and Andrew Zisserman. *Multiple view geometry in computer vision*. Cambridge university press, 2003. 1, 2, 4, 6
- [12] Paul W Holland and Roy E Welsch. Robust regression using iteratively reweighted least-squares. *Communications in Statistics-theory and Methods*, 6(9):813–827, 1977. 2
- [13] Peter J Huber. Robust estimation of a location parameter. In *Breakthroughs in statistics: Methodology and distribution*, pages 492–518. Springer, 1992. 1, 2
- [14] Peter J Huber. *Robust statistics*. John Wiley & Sons, 2004. 1, 2, 5
- [15] Junfeng Jing, Tian Gao, Weichuan Zhang, Yongsheng Gao, and Changming Sun. Image feature information extraction for interest point detection: A comprehensive review. *IEEE Transactions on Pattern Analysis and Machine Intelligence*, 45(4):4694–4712, 2023. 1
- [16] Laurent Kneip and Paul Furgale. OpenGV: A unified and generalized approach to real-time calibrated geometric vision. In *2014 IEEE International Conference on Robotics and Automation (ICRA)*, pages 1–8. IEEE, 2014. 2, 3, 6
- [17] Laurent Kneip and Simon Lynen. Direct optimization of frame-to-frame rotation. In *Proceedings of the IEEE/CVF International Conference on Computer Vision*, pages 2352–2359, 2013. 3, 6
- [18] Laurent Kneip, Roland Siegwart, and Marc Pollefeys. Finding the exact rotation between two images independently of the translation. In *European Conference on Computer Vision*, pages 696–709, 2012. 1, 2, 3
- [19] H Christopher Longuet-Higgins. A computer algorithm for reconstructing a scene from two projections. *Nature*, 293(5828):133–135, 1981. 1, 2, 3
- [20] David G Lowe. Distinctive image features from scale-invariant keypoints. *International Journal of Computer Vision*, 60:91–110, 2004. 1, 7
- [21] Pierre Moulon, Pascal Monasse, and Renaud Marlet. Adaptive structure from motion with a contrario model estimation. In *Asian Conference on Computer Vision*, pages 257–270. Springer, 2013. 2
- [22] Pierre Moulon, Pascal Monasse, Romuald Perrot, and Renaud Marlet. Openmvg: Open multiple view geometry. In *Reproducible Research in Pattern Recognition*, pages 60–74, 2017. 1, 2
- [23] David Nistér. An efficient solution to the five-point relative pose problem. *IEEE Transactions on Pattern Analysis and Machine Intelligence*, 26(6):756–770, 2004. 1, 2, 5

- [24] Onur Özyeşil, Vladislav Voroninski, Ronen Basri, and Amit Singer. A survey of structure from motion. *Acta Numerica*, 26:305–364, 2017. [1](#), [2](#)
- [25] Liangzu Peng, Christian Kümmerle, and René Vidal. On the convergence of irls and its variants in outlier-robust estimation. In *Proceedings of the IEEE/CVF Conference on Computer Vision and Pattern Recognition (CVPR)*, pages 17808–17818, 2023. [1](#), [2](#), [4](#), [5](#), [7](#)
- [26] Johan Philip. A non-iterative algorithm for determining all essential matrices corresponding to five point pairs. *The Photogrammetric Record*, 15(88):589–599, 1996. [2](#), [6](#)
- [27] J. Philip. Critical point configurations of the 5-, 6-, 7-, and 8-point algorithms for relative orientation. Technical Report TRITA-MAT-1998-MA-13, KTH Royal Institute of Technology, 1998. [1](#), [2](#)
- [28] Oscar Pizarro, Ryan M Eustice, and Hanumant Singh. Relative pose estimation for instrumented, calibrated imaging platforms. In *DICTA*, pages 601–612, 2003. [1](#), [2](#), [5](#), [6](#)
- [29] Peter J Rousseeuw. Least median of squares regression. *Journal of the American Statistical Association*, 79(388):871–880, 1984. [1](#), [2](#)
- [30] Ethan Rublee, Vincent Rabaud, Kurt Konolige, and Gary Bradski. ORB: An efficient alternative to SIFT or SURF. In *Proceedings of the IEEE/CVF International Conference on Computer Vision*, pages 2564–2571, 2011. [1](#)
- [31] Johannes L Schonberger and Jan-Michael Frahm. Structure-from-motion revisited. In *Proceedings of the IEEE/CVF Conference on Computer Vision and Pattern Recognition (CVPR)*, pages 4104–4113, 2016. [2](#)
- [32] Henrik Stewenius, Christopher Engels, and David Nistér. Recent developments on direct relative orientation. *ISPRS Journal of Photogrammetry and Remote Sensing*, 60(4):284–294, 2006. [1](#), [2](#), [5](#), [6](#), [7](#)
- [33] Richard Szeliski. *Computer vision: algorithms and applications*. Springer Nature, 2022. [1](#)
- [34] Ji Zhao. An efficient solution to non-minimal case essential matrix estimation. *IEEE Transactions on Pattern Analysis and Machine Intelligence*, 44(4):1777–1792, 2020. [2](#), [5](#), [6](#), [7](#), [9](#), [10](#)